

Supplemental Material for “Shear-Induced Migration of Confined Flexible Fibers”

Nan Xue,¹ Janine K. Nunes,¹ and Howard A. Stone^{1,*}

¹*Department of Mechanical and Aerospace Engineering,
Princeton University, Princeton, NJ 08544, USA*

(Dated: October 17, 2021)

Table S1. All the experimental conditions presented in this study. The table displays, respectively, the (series) number of the experiments (No.), the diameter of the fibers D , the gap size (the distance between the two parallel plates) d , the wait time (to achieve the initial conditions that the fibers sink to the bottom of the plate), the local shear rate in the field of view $\dot{\gamma}$, the effective fiber flexibility Λ_{eff} , the (series) numbers of the figures that display the experiments, the (series) numbers of the movies that show the experiments, the processing width (the fibers that move into the field of view from the center region in this width are measured and processed), and the remarks (whether additional water is added in the suspension).

Movies 1–30. The movies for experiments No. 1–15. The movies respectively show the fiber dynamics at the normalized time $\dot{\gamma}t = 0 - 50$ and $3950 - 4000$ in each experiment. An extended version of the movies ($\dot{\gamma}t = 0 - 1000$ and $3000 - 4000$, respectively) are available at <https://doi.org/10.34770/cp0y-ee27>.

Movie 31. The movie for demonstrating the dynamics of a bending fiber, in experiment No. 4, with $D = 44.8 \mu\text{m}$, $\dot{\gamma} = 105 \text{ s}^{-1}$, and $\Lambda_{\text{eff}} = 2 \times 10^3$.

Figure S1. The imaging of the fibers using the rheo-microscopy setup. The refractive index of the fibers is very close to the ambient liquid. To enhance the contrast of the image, the focal plane is either above [Fig. S1(c)] or below [Fig. S1(a)] the fiber suspension.

Figure S2. The demonstration of the measurements of the fibers. The orientations and end-to-end lengths of the fibers are measured when the fibers are at (close to) the vertical centerline of the field of view, where the dynamics of the fibers are not changing significantly. We note that tracking the orientations and end-to-end lengths of the fibers (while the fibers are in the field of view) would lead to a more accurate presentation of the behaviors of the fibers. However, this method of tracking is not applied in this work, and only one value of the orientation and end-to-end length is measured for each fiber. We also note that the conical shapes at the two ends of the fibers induce moderate errors in the experimental measurements.

Figure S3. A demonstration of the dynamics of a bending fiber. A large diameter fiber with the shear rate $\dot{\gamma} = 105 \text{ s}^{-1}$ and the effective flexibility $\Lambda_{\text{eff}} = 2 \times 10^3$ is used as an example. The end-to-end vector of the fiber is tracked. The mean velocity of the fiber u remains constant when the fiber does not bend. However, when the fiber bends, u rapidly changes in time, indicating that the vertical position of the fiber z also changes during the bending. This observation demonstrates that the vertical position of the fiber z changes when the fiber bends, which implies that the fiber drifts normal to the walls during the bending dynamics.

Figure S4. The distribution of the alignment angles $|\theta|$ and the end-to-end lengths L_{ee} of the fibers. The comparison shows distinct differences in the distributions with different effective flexibilities Λ_{eff} . The standard error of the data is calculated by $(\sum_i w_i'^2 \sigma_i^2)^{1/2}$, where $w_i' = w_i / \sum_i w_i$ is the normalized weight function (the weight function w_i is the transit time that the fiber is in the field of view) of the fiber i , σ_i is the deviation (to the mean value) of the fiber i . The standard deviation of the data is calculated by $(\sum_i w_i' \sigma_i^2)^{1/2}$.

Figure S5. The shear-induced migration of small diameter fibers. This figure is a small-diameter-fiber version of Fig. 4(a) in the article.

Figures S6–S19 The migration of the fibers in shear flows. These figures are similar plots to Figs. 2(d,e) in the article but with different experimental conditions.

Figure S20. A comparison of the fiber distributions during the migration in the shear flows, with the same shear rate $\dot{\gamma} = 105 \text{ s}^{-1}$, the gap sizes $d = 0.5$ and 1.5 mm , and with or without adding 10 vol% water into the suspension (to enhance the density difference). As a result, the migration is very similar while the velocities of the fibers are normalized by $u_0 = \dot{\gamma}d$. Therefore, with this shear rate, the buoyancy effect is negligible. Also, the fibers are confined between the plates, but the gap size does not significantly affect the normalized migration time scale. (However, we

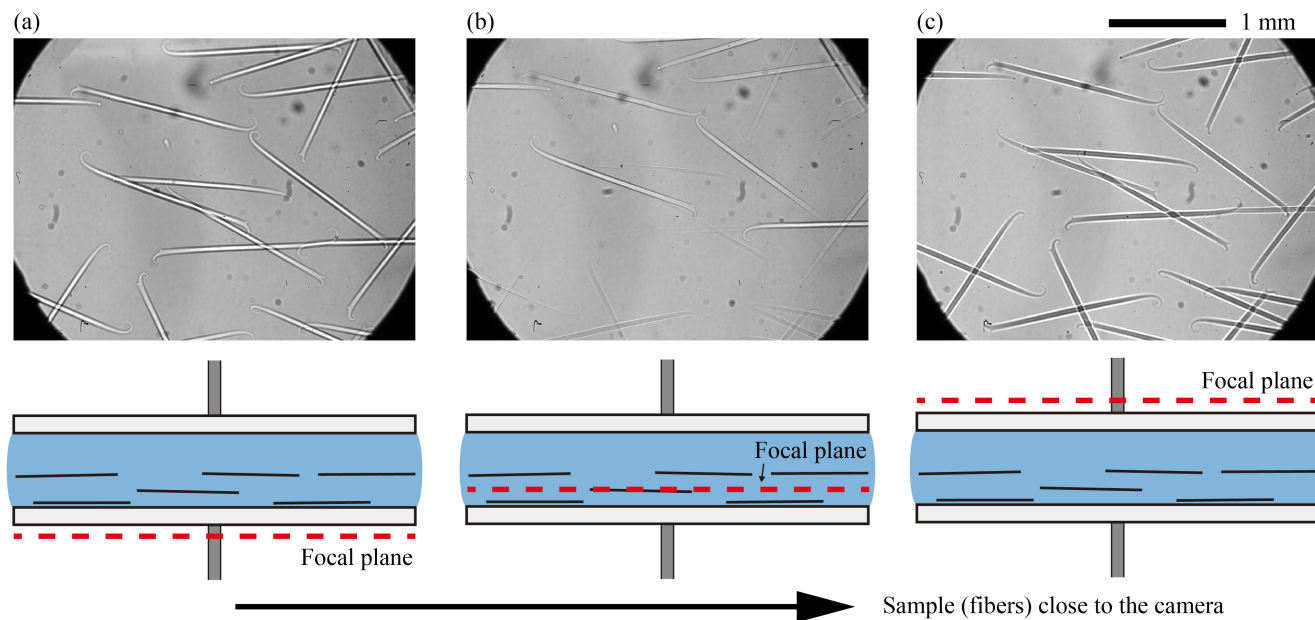


FIG. 1. The imaging of the fibers using a rheo-macroscopy setup. In this demonstration, the positions of the focal plane are, respectively, (a) below the fibers, (b) in (near the center of) the fibers, and (c) above the fibers. Note that in this demonstration, the fibers have not fully settled to the bottom yet, and the camera is at the bottom of the setup (there is also a mirror that re-directs the LED light and is not drawn in the sketch).

note that the rolling and tumbling fibers indeed migrate slower with larger gap sizes.)

* hastone@princeton.edu

No.	D (μm)	d (mm)	Wait time (min)	$\dot{\gamma}$ (s^{-1})	Λ_{eff}	Figure No(s).	Movie No(s).	Processing width (pixels)	Remarks
1	44.8	0.5	15	1	2×10^1	3(a), S2(a), and S6	1 and 2	200	-
2	44.8	0.5	15	5	1×10^2	S7	3 and 4	600	-
3	44.8	0.5	15	21	4×10^2	3(b) and S8	5 and 6	600	-
4	44.8	0.5	15	105	2×10^3	2, S2(b), S3(b), and S20	7 and 8	600	-
5	44.8	0.5	15	209	4×10^3	S9	9 and 10	200	-
6	44.8	0.5	15	523	1×10^4	3(c) and S10	11 and 12	200	-
7	44.8	0.5	15	1047	2×10^4	S2(a) and S11	13 and 14	200	-
8	23.3	0.5	45	1	3×10^2	S12	15 and 16	50	-
9	23.3	0.5	45	5	1×10^3	3(d) and S13	17 and 18	50	-
10	23.3	0.5	45	21	5×10^3	S14	19 and 20	50	-
11	23.3	0.5	45	105	3×10^4	3(e) and S15	21 and 22	50	-
12	23.3	0.5	45	523	1×10^5	S16	23 and 24	50	-
13	23.3	0.5	45	2093	5×10^5	3(f) and S17	25 and 26	50	-
14	44.8	1.5	45	105	2×10^3	S18 and S20	27 and 28	50	-
15	44.8	1.5	45	105	2×10^3	S19 and S20	29 and 30	50	10% water

TABLE I. The conditions of the experiments and the corresponding series of figures and movies.

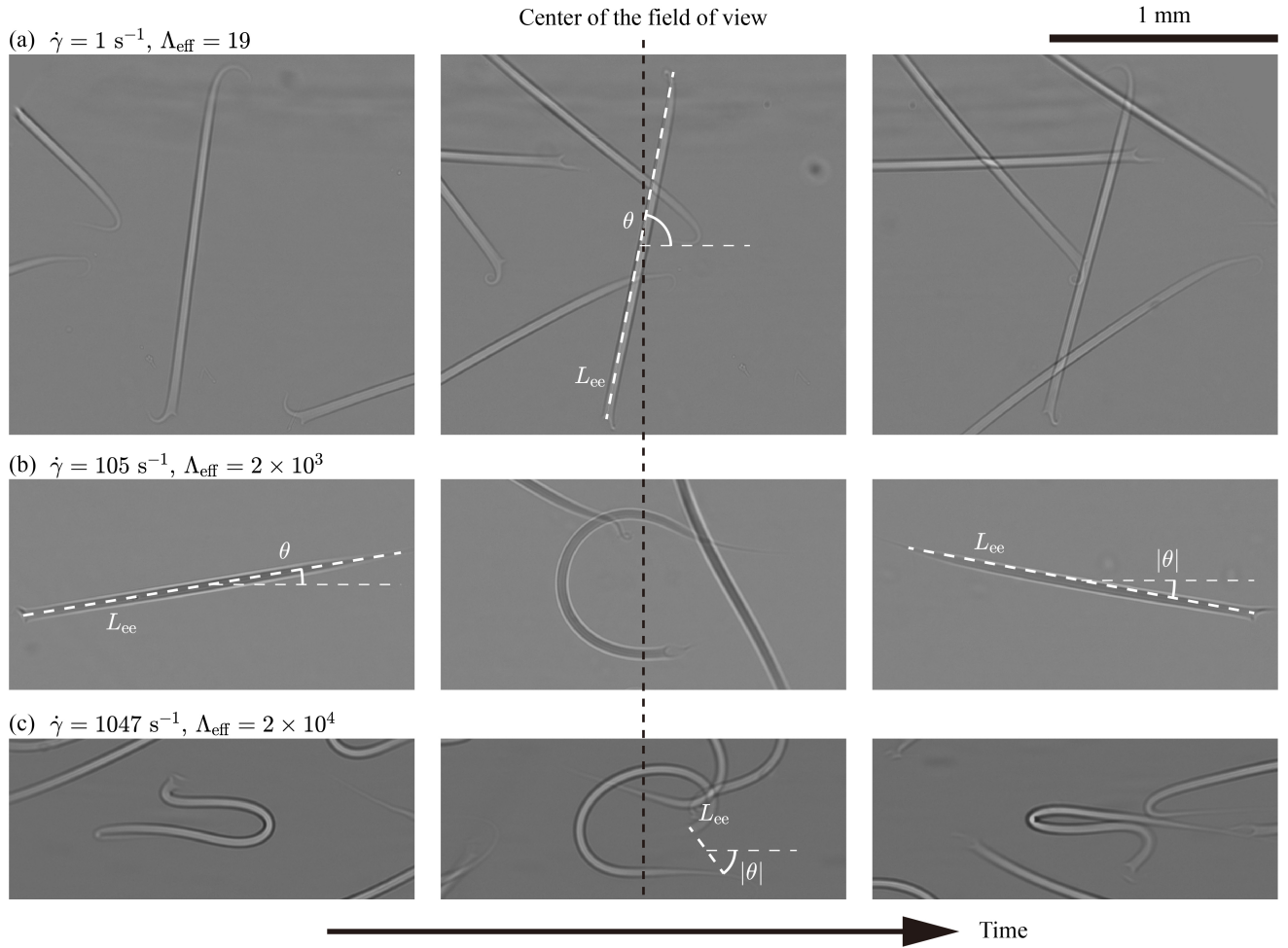


FIG. 2. The demonstration of the measurements of the fibers. Here the fibers have large diameters ($D = 44.8 \mu\text{m}$). The measurements of the orientations and end-to-end lengths of the fibers are performed when the fibers are at (close to) the vertical centerline of the field of view where the dynamics are relatively consistent. (a) At a relatively low shear rate, the fibers are not observed bent and the fibers only roll or tumble. The fibers are measured when the fibers are at the vertical centerline of the field of view. (b) At a moderate shear rate, seldomly, the fibers might bend when they are at the vertical centerline of the field of view. We note that the fibers are straight and not bent the majority of the time. To better demonstrate the re-orientations of the fibers under the shear flow, we measure the fiber while it remains stable (i.e., when the fiber does not change the orientation rapidly). (c) At a high shear rate, the fibers are bent most of the time, and the fibers are measured when the fibers are at the vertical centerline of the field of view.

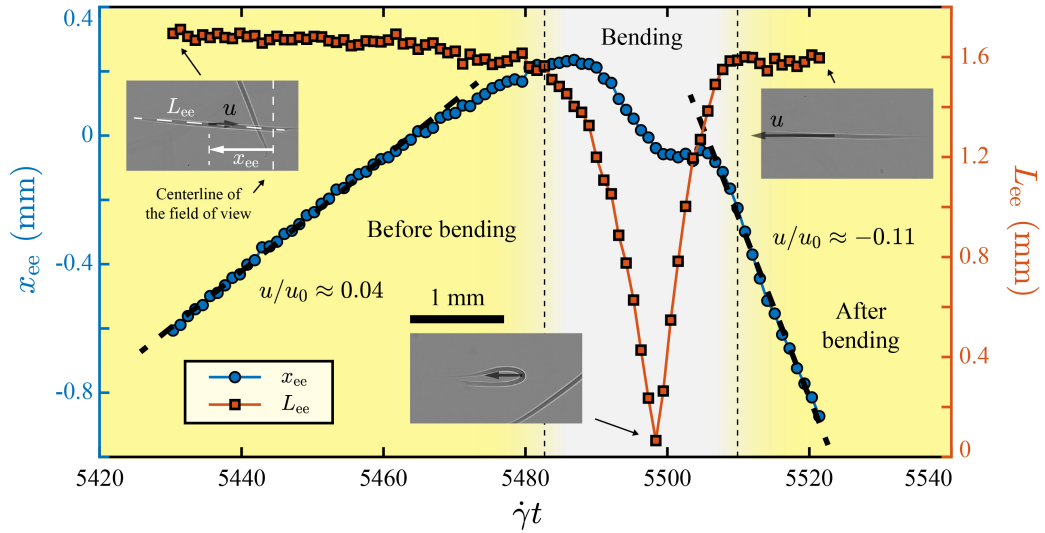


FIG. 3. A demonstration of the dynamics of a bending fiber. A large diameter fiber with the shear rate $\dot{\gamma} = 105 \text{ s}^{-1}$ and the effective flexibility $\Lambda_{\text{eff}} = 2 \times 10^3$ is used as an example. The end-to-end vector of the fiber is tracked. The blue circles (left y-axis) show the position of the center of the end-to-end vector in the flow direction x_{ee} as a function of the normalized time $\hat{\gamma}t$ ($x_{ee} = 0$ denotes the centerline of the field of view and positive x_{ee} indicates that the fiber is in the right part of the field of view). The red squares (right y-axis) show the end-to-end length of the fiber L_{ee} as a function of $\hat{\gamma}t$. When the fiber does not bend, x_{ee} linearly increases or decreases, indicating that the fiber has a constant speed u and therefore a constant vertical position z between the two plates. In contrast, when the fiber bends, L_{ee} rapidly decreases in time and then increases, and the mean velocity of the fiber u changes during the bending. The difference of the mean velocity of the fiber between before and after the bending dynamics indicates that the vertical position of the fiber z changes during the bending. This observation implies that the fiber drifts normal to the walls when bending occurs. The corresponding movie for the demonstration is Movie 31.

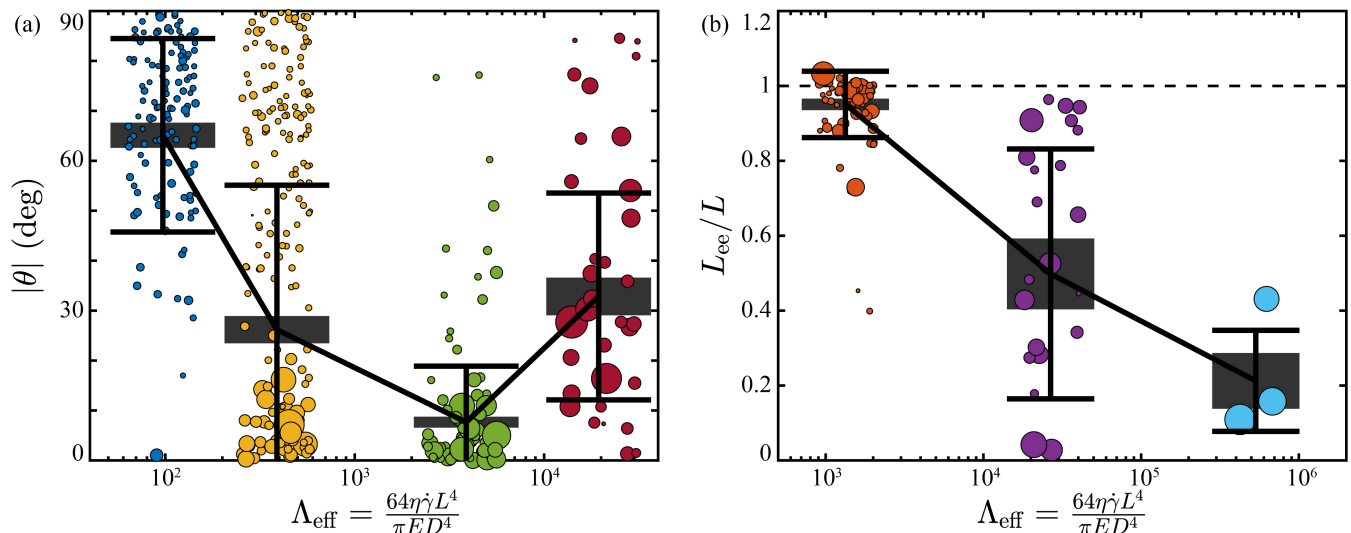


FIG. 4. The distribution of the alignment angles and end-to-end lengths of the measured fibers. (a) The distribution of the alignment angles of the fibers $|\theta|$ as a function of the effective flexibility Λ_{eff} . The fibers have large diameters $D = 44.8 \mu\text{m}$. The conditions of the experiments are, respectively, $\dot{\gamma} = 5 \text{ s}^{-1}$ and $\Lambda_{\text{eff}} = 1 \times 10^2$ (blue), $\dot{\gamma} = 21 \text{ s}^{-1}$ and $\Lambda_{\text{eff}} = 4 \times 10^2$ (yellow), $\dot{\gamma} = 209 \text{ s}^{-1}$ and $\Lambda_{\text{eff}} = 4 \times 10^3$ (green), and $\dot{\gamma} = 1047 \text{ s}^{-1}$ and $\Lambda_{\text{eff}} = 2 \times 10^4$ (crimson). (b) The distribution of the normalized end-to-end lengths of the fibers L_{ee}/L as a function of the effective flexibility Λ_{eff} . The fibers have small diameters $D = 23.3 \mu\text{m}$. The conditions of the experiments are, respectively, $\dot{\gamma} = 5 \text{ s}^{-1}$ and $\Lambda_{\text{eff}} = 1 \times 10^3$ (red-orange), $\dot{\gamma} = 104 \text{ s}^{-1}$ and $\Lambda_{\text{eff}} = 3 \times 10^4$ (purple), and $\dot{\gamma} = 2093 \text{ s}^{-1}$ and $\Lambda_{\text{eff}} = 5 \times 10^5$ (cyan). The displayed data are the measurements from the normalized time $\dot{\gamma}t = 2000$ to 4000 and are jittered for visualization (i.e., a small amount of random noise was added to visualize overlapping data). The radii of the data points (circles) indicate (are proportional to) the transit times that the fibers are in the field of view, which are used as the weight function (w_i) in the statistical processing. The black lines respectively represent the average value of the alignment angle $\langle |\theta| \rangle$ and the end-to-end length $\langle L_{\text{ee}}/L \rangle$ of the fibers as a function of Λ_{eff} . The gray shaded areas represent the standard error of the data, and the error bars represent the standard derivation of the data.

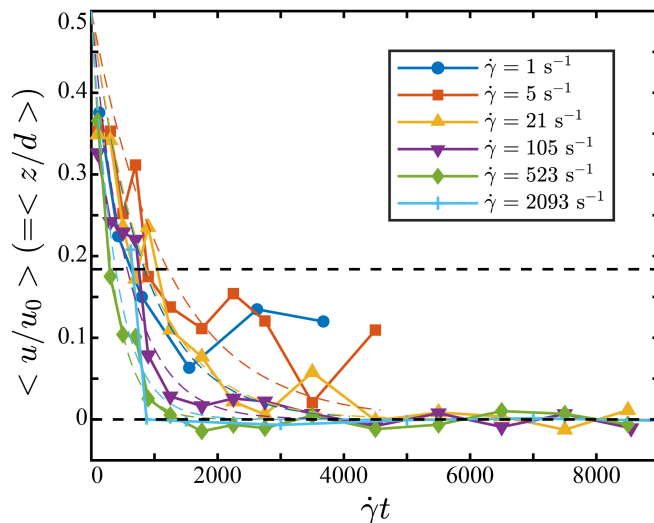


FIG. 5. The shear-induced migration of small diameter fibers. The normalized velocity of the fibers ($D = 23.3 \mu\text{m}$) $\langle u/u_0 \rangle$ as a function of the normalized time (shear strain) $\dot{\gamma}t$ is displayed. The shear rate of the flow $\dot{\gamma} = 1$ (circles), 5 (squares), 21 (upward-pointing triangles), 105 (downward-pointing triangles), 523 (diamonds), and 2093 (plus signs) s^{-1} , respectively. The corresponding effective flexibility $\Lambda_{\text{eff}} = 3 \times 10^2$, 1×10^3 , 5×10^3 , 3×10^4 , 1×10^5 , and 5×10^5 , respectively. The dashed line shows the corresponding fitting curve using the equation $u/u_0 = \frac{1}{2}e^{-\dot{\gamma}t/\tau_0}$, where τ_0 represents the typical normalized time scale of the shear-induced migration of the fibers.

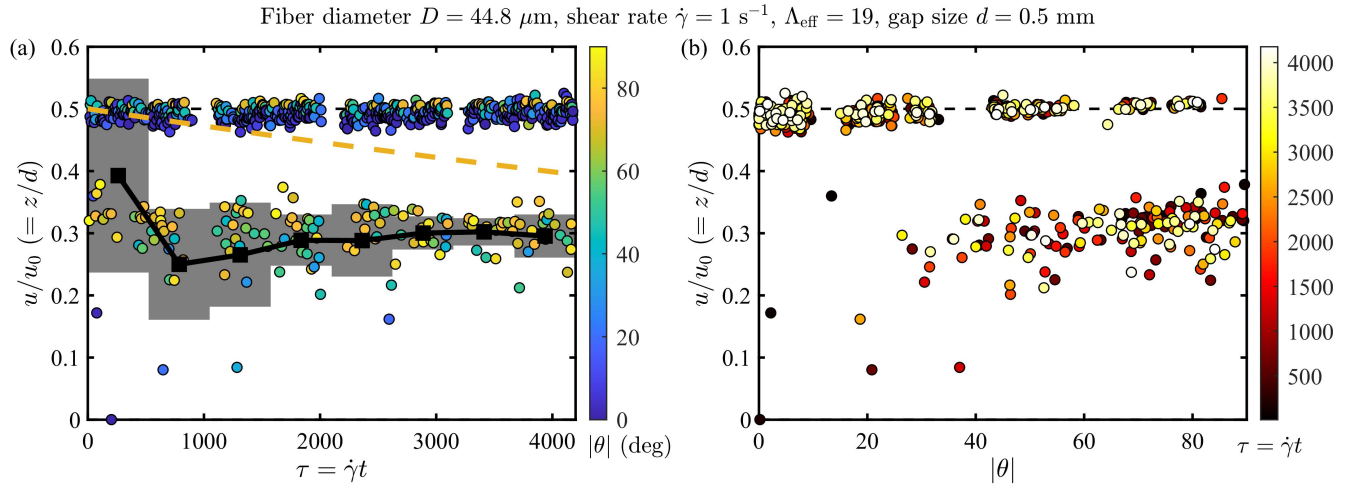


FIG. 6. The migration of fibers in a shear flow. The conditions of the experiment are on the top of the figures. The corresponding movies for the experiment are Movies 1 and 2.

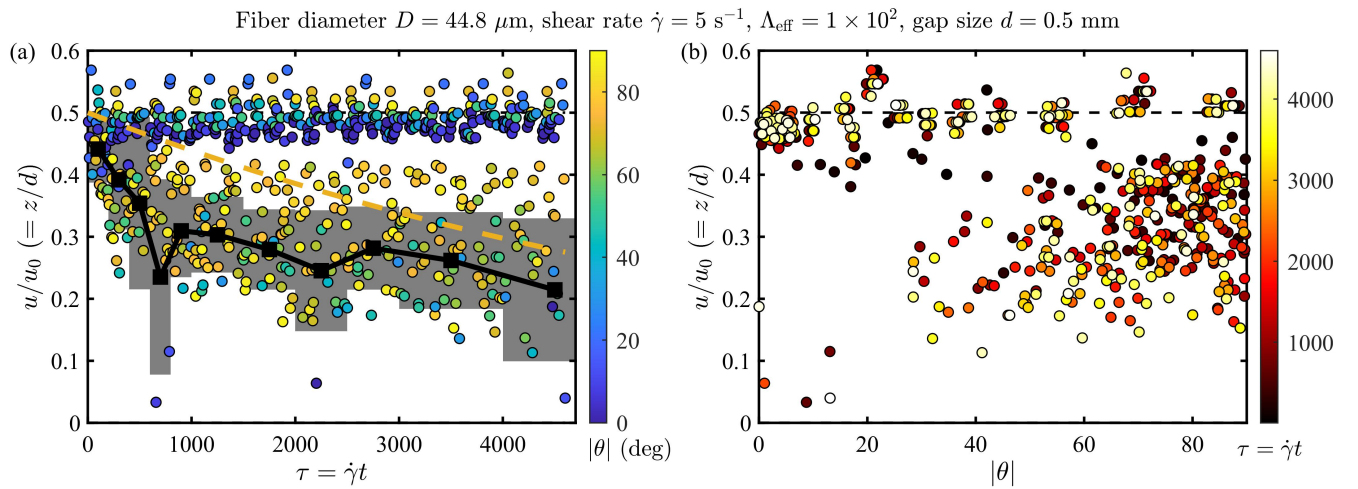


FIG. 7. The migration of fibers in a shear flow. The conditions of the experiment are on the top of the figures. The corresponding movies for the experiment are Movies 3 and 4.

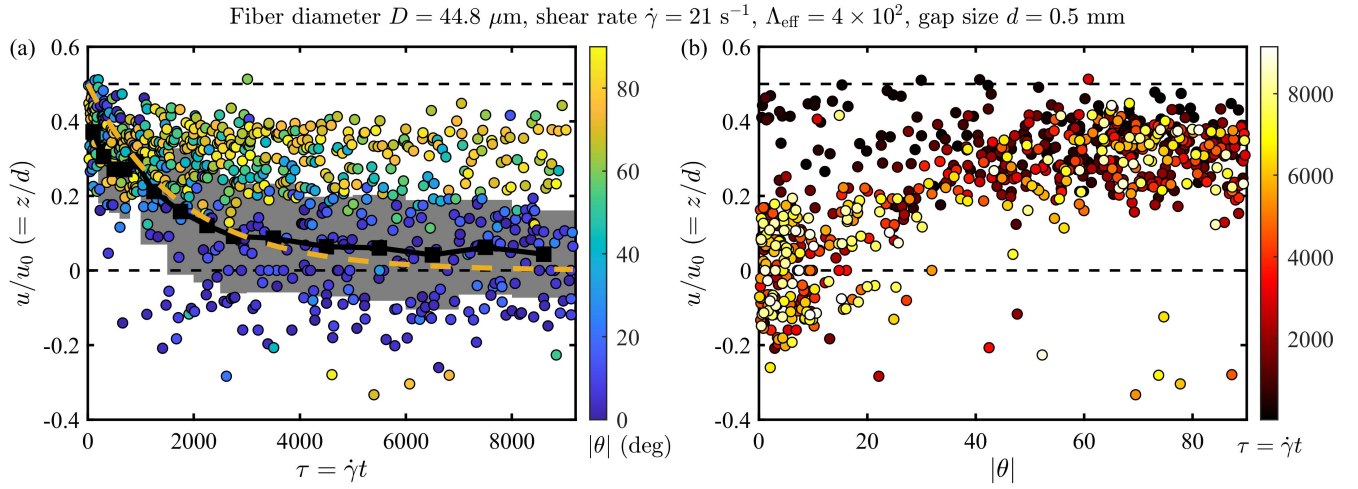


FIG. 8. The migration of fibers in a shear flow. The conditions of the experiment are on the top of the figures. The corresponding movies for the experiment are Movies 5 and 6.

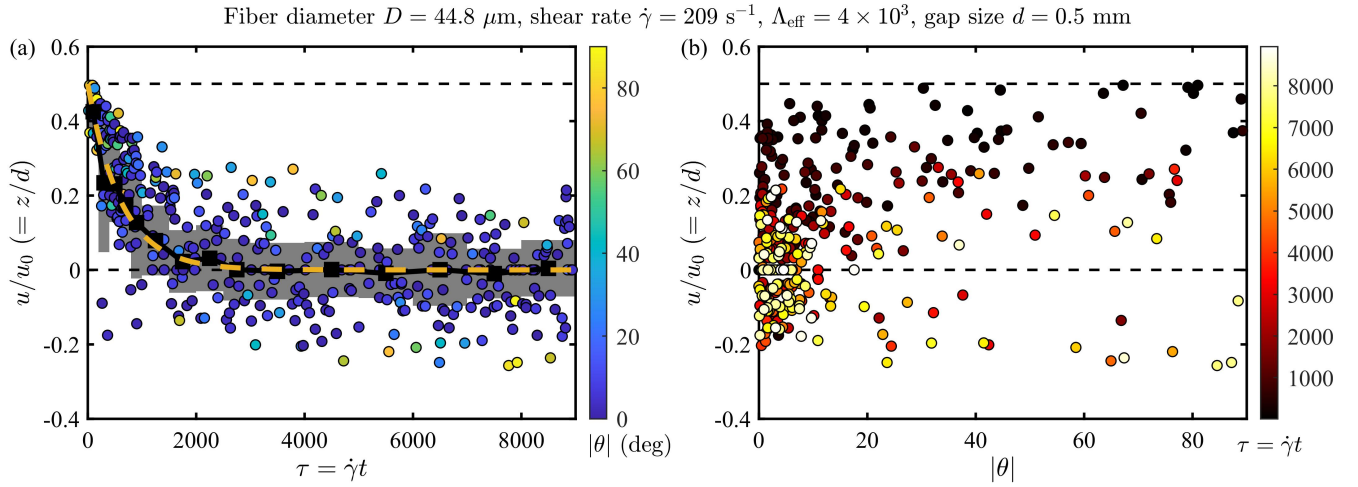


FIG. 9. The migration of fibers in a shear flow. The conditions of the experiment are on the top of the figures. The corresponding movies for the experiment are Movies 9 and 10.

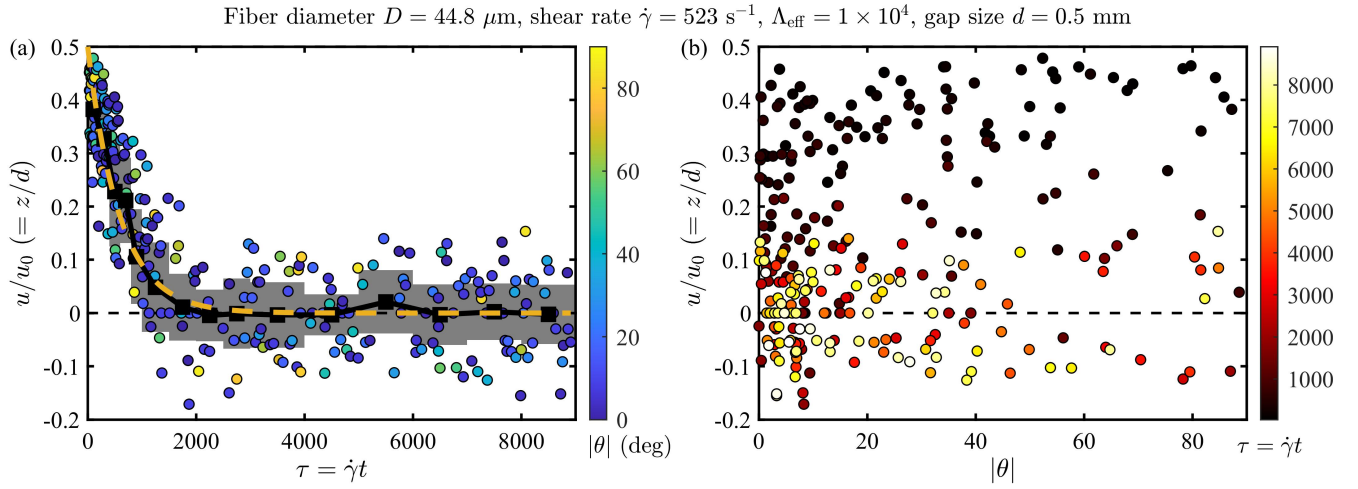


FIG. 10. The migration of fibers in a shear flow. The conditions of the experiment are on the top of the figures. The corresponding movies for the experiment are Movies 11 and 12.

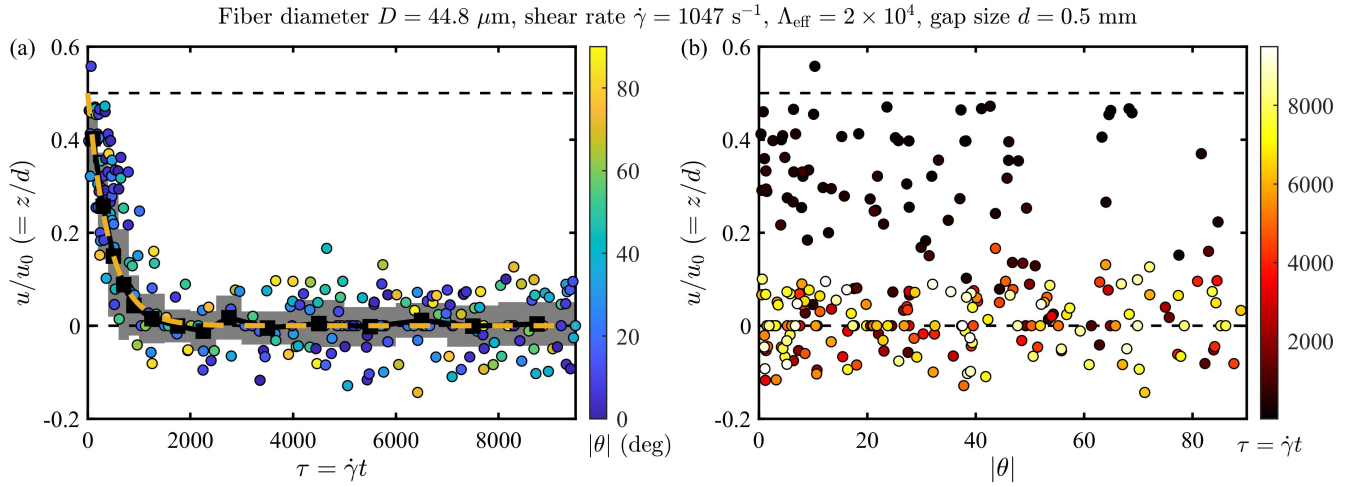


FIG. 11. The migration of fibers in a shear flow. The conditions of the experiment are on the top of the figures. The corresponding movies for the experiment are Movies 13 and 14.

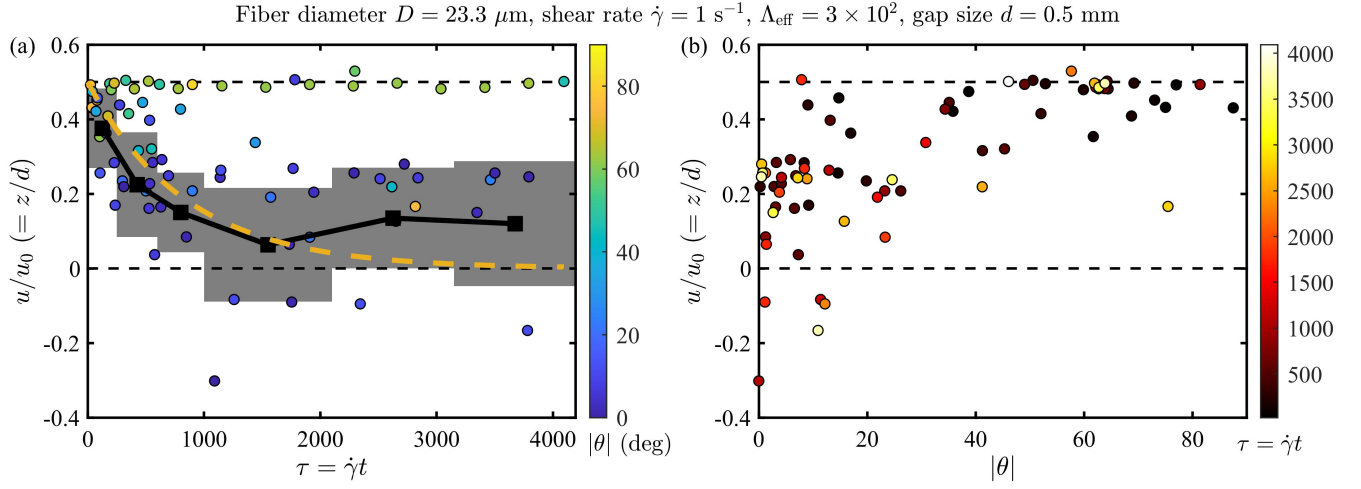


FIG. 12. The migration of fibers in a shear flow. The conditions of the experiment are on the top of the figures. The corresponding movies for the experiment are Movies 15 and 16.

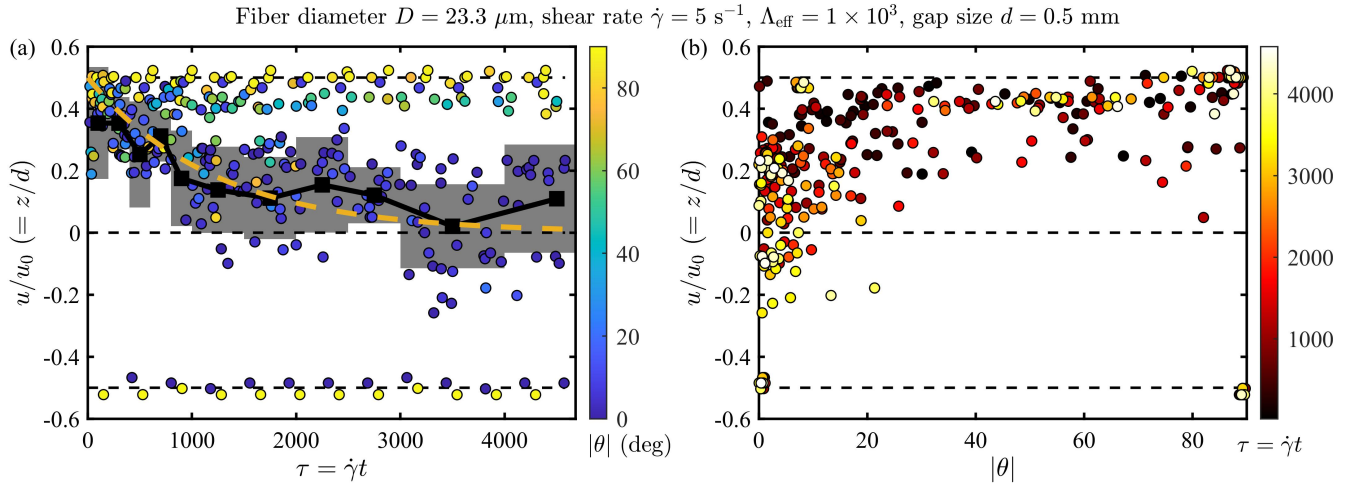


FIG. 13. The migration of fibers in a shear flow. The conditions of the experiment are on the top of the figures. The corresponding movies for the experiment are Movies 17 and 18.

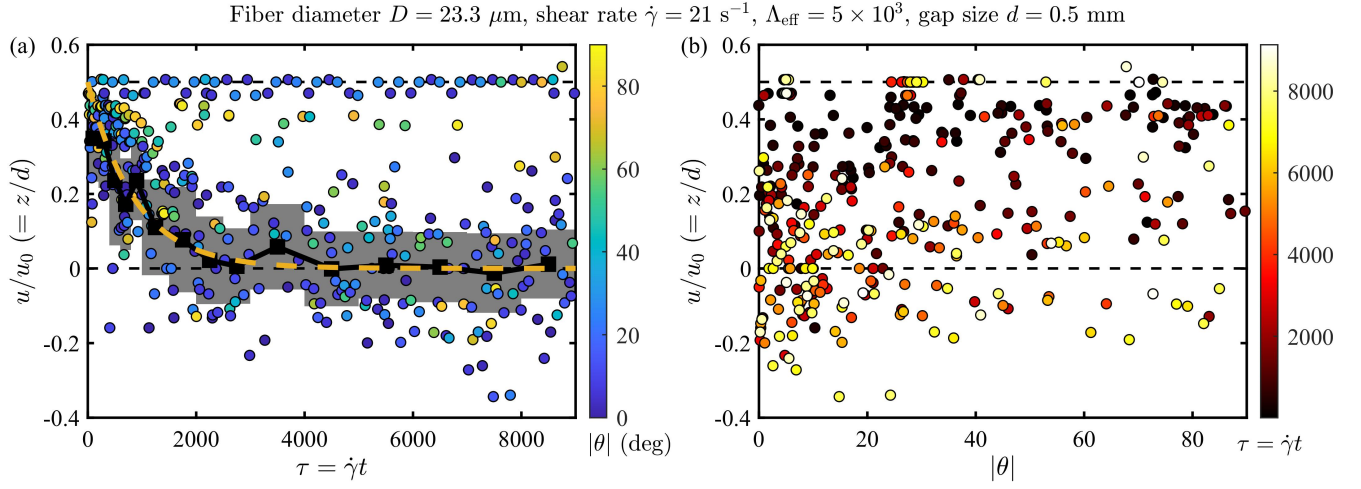


FIG. 14. The migration of fibers in a shear flow. The conditions of the experiment are on the top of the figures. The corresponding movies for the experiment are Movies 19 and 20.

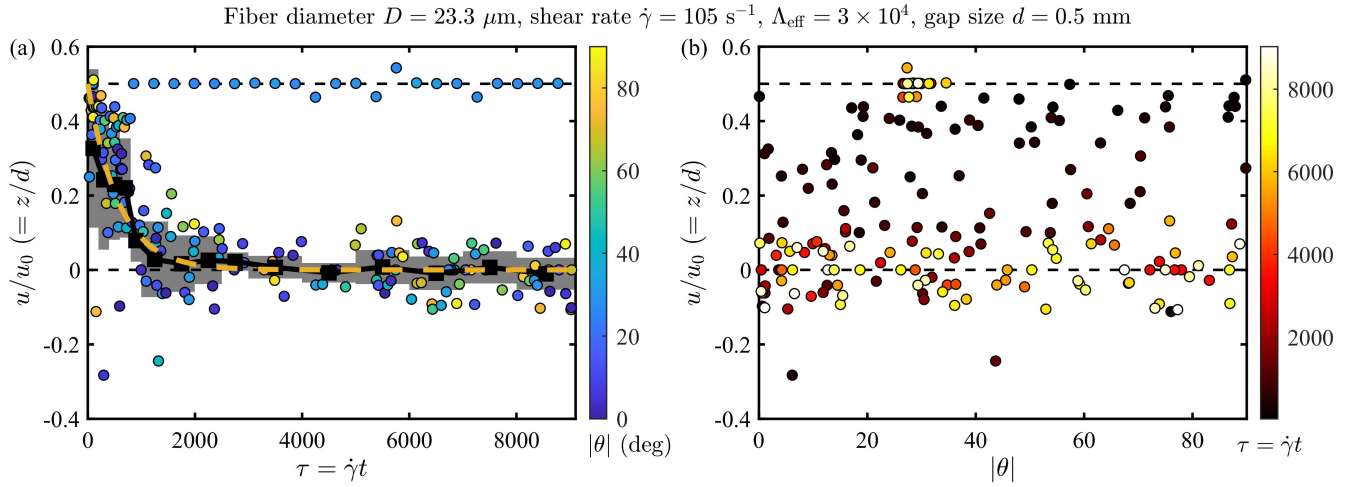


FIG. 15. The migration of fibers in a shear flow. The conditions of the experiment are on the top of the figures. The corresponding movies for the experiment are Movies 21 and 22.

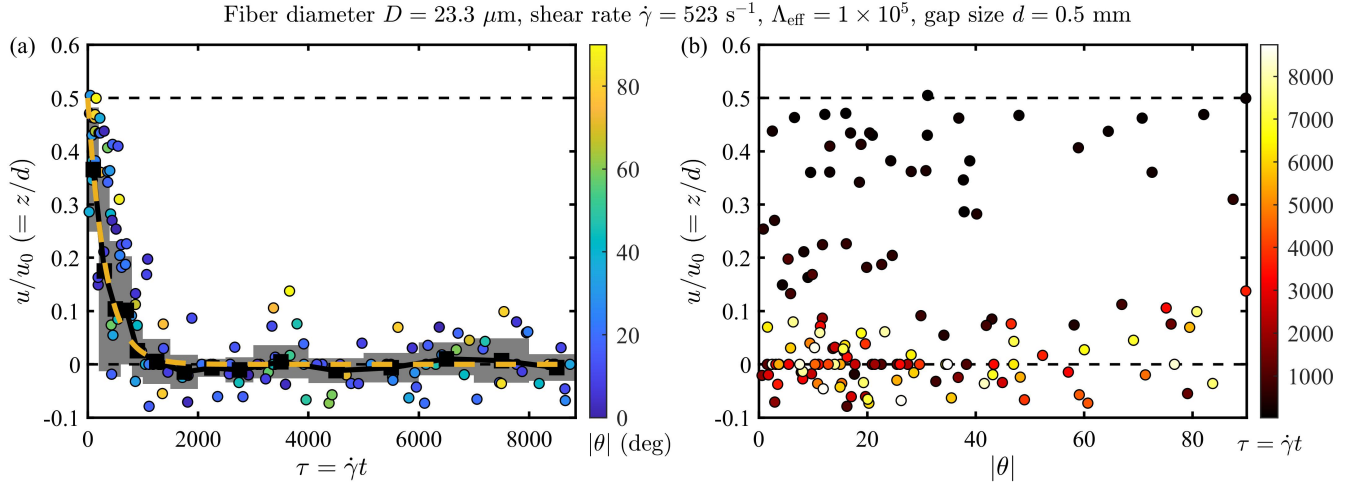


FIG. 16. The migration of fibers in a shear flow. The conditions of the experiment are on the top of the figures. The corresponding movies for the experiment are Movie 23 and 24.

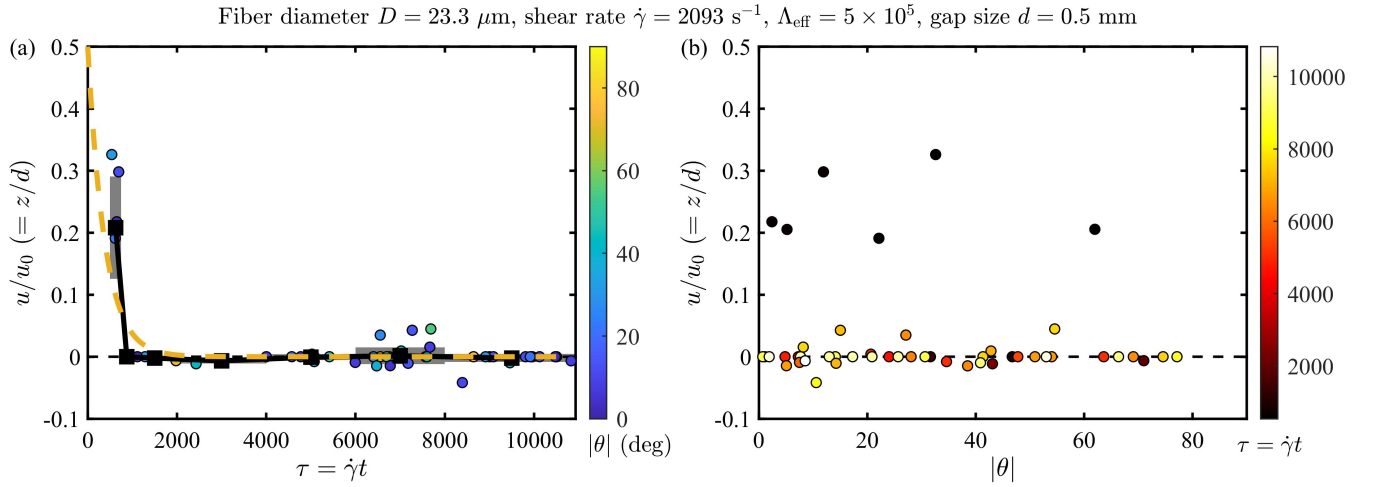


FIG. 17. The migration of fibers in a shear flow. The conditions of the experiment are on the top of the figures. The corresponding movies for the experiment are Movies 25 and 26.

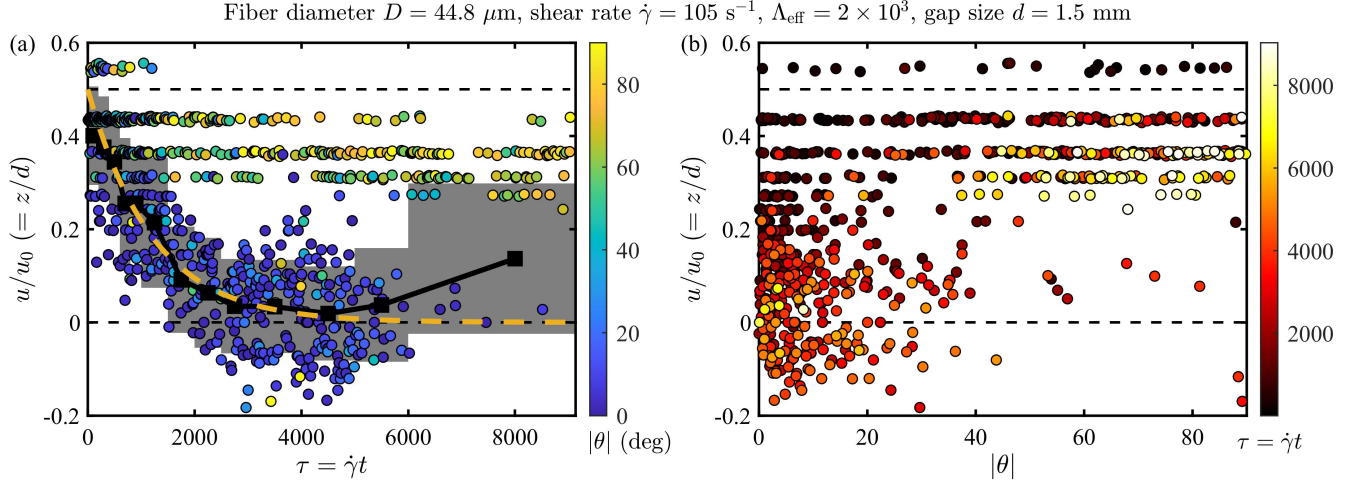


FIG. 18. The migration of fibers in a shear flow. The conditions of the experiment are on the top of the figures. The corresponding movies for the experiment are Movies 27 and 28.

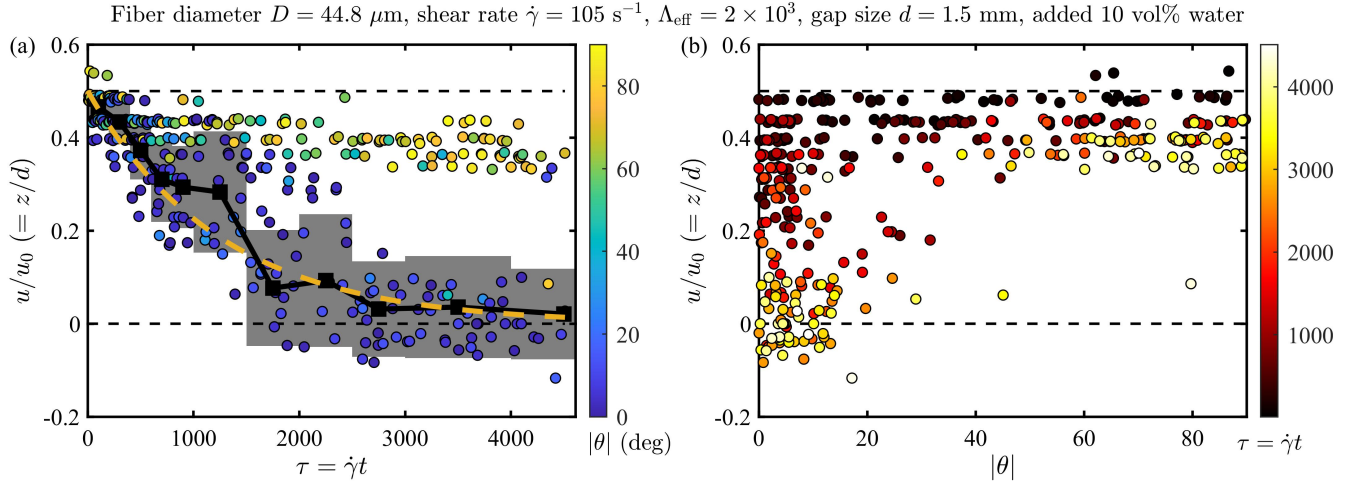


FIG. 19. The migration of fibers in a shear flow. The conditions of the experiment are on the top of the figures. The corresponding movies for the experiment are Movies 29 and 30.

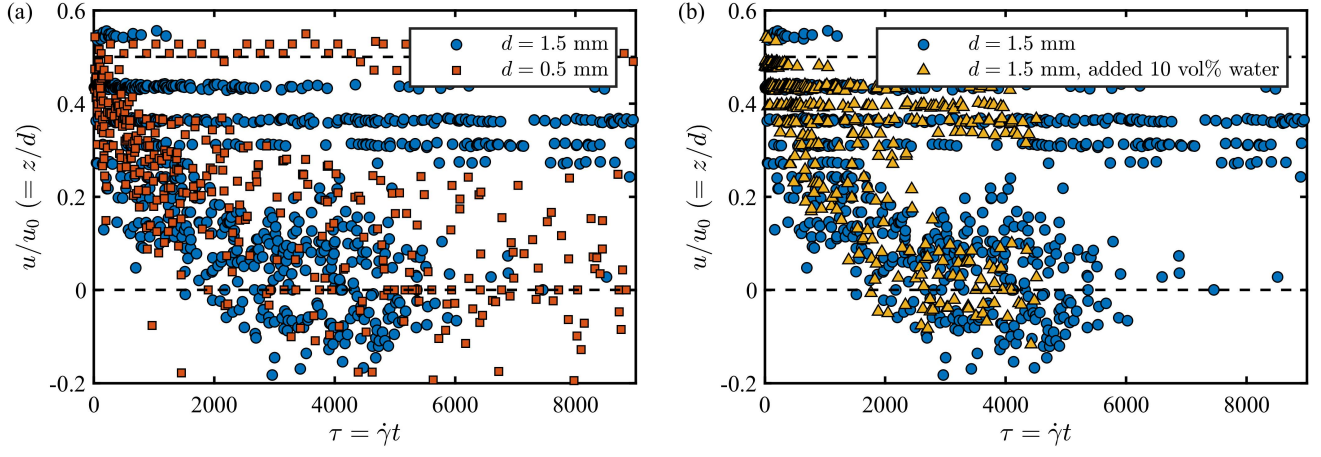


FIG. 20. A comparison of the fiber distributions during the migration in shear flows. The shear rate $\dot{\gamma} = 105 \text{ s}^{-1}$. (a) The comparison between the experiments with the gap sizes $d = 0.5$ and 1.5 mm. (a) The comparison between the experiments with and without adding 10 vol% water into the suspension.